

Comparing EAM Potentials to Model Slip Transfer of Sequential Mixed Character Dislocations Across Two Symmetric Tilt Grain Boundaries in Ni

SHUOZHI XU,¹ LIMING XIONG,² YOUNPING CHEN,³
and DAVID L. MCDOWELL^{1,4,5}

1.—Woodruff School of Mechanical Engineering, Georgia Institute of Technology, Atlanta, GA 30332-0405, USA. 2.—Department of Aerospace Engineering, Iowa State University, Ames, IA 50011, USA. 3.—Department of Mechanical and Aerospace Engineering, University of Florida, Gainesville, FL 32611-6250, USA. 4.—School of Materials Science and Engineering, Georgia Institute of Technology, Atlanta, GA 30332-0245, USA. 5.—e-mail: david.mcdowell@me.gatech.edu

Slip transfer via sequential pile-up dislocations across grain boundaries (GBs) plays an important role in plastic deformation in polycrystalline face-centered cubic (FCC) metals. In this work, large scale concurrent atomistic-continuum (CAC) method simulations are performed to address the slip transfer of mixed character dislocations across GBs in FCC Ni. Two symmetric tilt GBs, a $\Sigma_3\{111\}$ coherent twin boundary (CTB) and a $\Sigma_{11}\{113\}$ symmetric tilt GB (STGB), are investigated using five different fits to the embedded-atom method (EAM) interatomic potential to assess the variability of predicted dislocation-interface reaction. It is shown that for the Σ_3 CTB, two of these potentials predict dislocation transmission while the other three predict dislocation absorption. In contrast, all five fits to the EAM potential predict that dislocations are absorbed by the Σ_{11} STGB. Simulation results are examined in terms of several slip transfer criteria in the literature, highlighting the complexity of dislocation/GB interactions and the significance of multiscale modeling of the slip transfer process.

INTRODUCTION

Grain boundaries (GBs) play a fundamental role in size-dependent mechanical properties of metals.¹ In polycrystalline face-centered cubic (FCC) metals subjected to an applied shear stress, a series of dislocations in a single pile-up move through a lattice in individual grains until encountering a GB.^{2,3} In general, as more dislocations add to the end of the pile-up, the leading dislocation experiences a higher stress, which is eventually large enough for the tip of the pile-up to react with the GB, lowering the overall stress and allowing further deformation of the material if the dislocation is transmitted or absorbed and desorbed. As such, a larger grain accommodating a larger number of dislocations requires a lower applied stress to “yield” the GBs in a polycrystal, manifesting a Hall–Petch effect. Direct studies of sequential incoming lattice dislocations interacting with GBs

at the sub-micron scale are important, as results can't be simply extrapolated from atomistic simulations involving only an isolated, short, straight dislocation segment.⁴

Although *in situ* TEM experiments capture the real-time dynamic process of slip transfer,⁵ they are unable to discern 3D atomic-scale events at the dislocation/GB interaction sites to yield quantitative information.⁶ The multiscale nature of the sequential transfer of slip across GBs, in which both the atomic scale structure of the interface and the long range fields of dislocation pile-ups are important, also poses challenges from the perspective of computational simulation.⁷ For example, dislocation-based continuum approaches such as the crystal plasticity finite element method⁷ and rule-based dislocation dynamics⁸ are not readily applicable to simulate the interactions between dislocations and GBs because they usually do not naturally incorporate the necessary microscopic degrees of freedom

(DOFs) associated with the GBs and other evolving internal state variables that relate to detailed slip transfer criteria. On the other hand, atomistic simulations, which are preferred to understand local GB structure-specific slip transfer responses, are limited by the size of the computational cell in considering the long-range stress field associated with the dislocation pile-up processes.⁴

Therefore, multiscale simulation approaches are warranted to facilitate parametric studies of dislocation/GB reactions concerning a wide range of dislocations and GBs with the same computational resources.² Concurrent multiscale modeling of dislocation-interface reactions has been pursued using the coupled atomistic and discrete dislocation (CADD) method^{9,10} and the quasicontinuum (QC) method,¹¹ the latter study revealing that reversing the Burgers vector of an edge dislocation on a given slip plane significantly changes its interactions with a $\Sigma 11\langle 112 \rangle\{113\}$ GB in Cu.

In this work, we perform concurrent atomistic-continuum (CAC) simulations² to study the sequential slip transfer of mixed character dislocations for two symmetric GBs in FCC Ni: a $\Sigma 3\langle 110 \rangle\{111\}$ coherent twin boundary (CTB) and a $\Sigma 11\langle 110 \rangle\{113\}$ symmetric tilt GB (STGB). In CAC simulations, interface reactions are described using fully resolved atomistics while the net Burgers vector and associated long range stress fields of dislocations in a pile-up are preserved in a fully 3D model.¹² The CAC approach avoids essential remeshing operations, and criteria/procedures for passing dislocation segments between atomistic and coarse-grained domains.^{13,14} The success of our early calculations, including dislocation/void interactions in Ni,¹⁵ dislocation/CTB interactions in Cu and Al,² fast moving dislocations in Cu,¹⁶ screw dislocation cross-slip in Ni,¹⁷ dislocations bowing out from obstacles in Al,¹⁸ and dislocation multiplication from Frank–Read sources in Cu, Ni, an Al,¹⁹ suggests the viability of using CAC simulations in the context of sequential slip transfer across GBs with greatly reduced DOFs relative to full atomistic simulations.

We focus on a $\Sigma 3\langle 111 \rangle$ CTB and a $\Sigma 11\langle 113 \rangle$ STGB because they have the simplest GB structure and lowest GB energy among all STGBs with a common $\langle 110 \rangle$ misorientation axis.²⁰ CADD simulations for pure Al showed that while a series of straight pure screw dislocations are absorbed by both $\Sigma 3\langle 111 \rangle$ CTB and $\Sigma 11\langle 113 \rangle$ STGB,⁹ a mixed character dislocation pile-up is transmitted across both boundaries.¹⁰ In Ni, QC and atomistic simulations revealed that (1) a single pure screw dislocation may be transmitted across or absorbed by a $\Sigma 3$ CTB, depending on the interatomic potential adopted,^{21,22} (2) a single mixed type dislocation is transmitted across a $\Sigma 3$ CTB,²³ and (3) a single pure edge dislocation is transmitted across a $\Sigma 11\langle 113 \rangle$ STGB.²⁴ Nevertheless, the sensitivity of the modeled response of a mixed character dislocation pile-up impingement against these two boundaries to

the interatomic potential for Ni remains to be addressed. We also attempt to shed light on slip transfer criteria in the literature. For example, Sangid et al.²⁰ proposed that the energy barrier to direct transmission of a dislocation across a GB is inversely related to the excess energy for each GB; in particular for the $\Sigma 3$ CTB, based on certain material properties such as the stacking and twinning fault energies, Jin et al.²² and Chassagne et al.²¹ proposed different criteria (discussed in detail in the RESULTS AND DISCUSSIONS section) to discriminate between dislocation transmission and absorption in screw dislocation/CTB interactions. In this paper, we will study the applicability of these criteria, along with uncertainty in computed dislocation-interface reactions associated with the deployment of a variety of interatomic potentials for Ni.^{25–29}

MATERIALS AND METHODS

For both $\Sigma 3\langle 111 \rangle$ CTB and $\Sigma 11\langle 113 \rangle$ STGB, an atomistic domain is meshed in the vicinity of GBs to naturally accommodate GB structure evolution at the atomic scale, as shown in Fig. 1. All simulation cell boundaries are assumed traction free to allow a full 3D description. Equilibrium structures at 0 K of the GBs are determined through energy minimization,² which also provides the equilibrium lattice parameter which potentially plays an important role in stacking fault energies (SFEs)³⁰ and dislocation/GB interactions. The $\Sigma 3$ CTB is composed of all D structural units (SUs), while the $\Sigma 11$ STGB is composed of all C SUs. As such, only one dislocation impingement site is considered for the $\Sigma 3$ CTB while two distinct sites are for the $\Sigma 11$ STGB. In the coarse-grained domain, 3D rhombohedral second nearest neighbor elements are employed with surfaces corresponding to $\{111\}$ slip planes.^{14,31,32} Five straight, equidistant, pure screw dislocations in a single pile-up, each of which has a Burgers vector $\mathbf{b} = \frac{1}{2}\mathbf{a}_0[110]$, are introduced on the mid plane normal to the z axis.²² A shear stress is then applied on the simulation cell to drive the dislocation pile-up toward the GBs. This is accomplished by imposing a zx shear deformation on the simulation cell as necessary to maintain a constant remote average shear stress. The lower boundary is fixed in the x direction, while the upper boundary is displaced along the positive x direction (boundaries are normal to the z axis). All nodes and atoms between the upper and lower boundaries are displaced linearly in the x direction. More details regarding the quasistatic CAC method and its numerical implementation,¹⁴ application to dislocation-interface reactions,² and visualization^{33–37} are summarized in Supplementary Materials.

Five embedded-atom method (EAM) potentials, by Mishin et al.²⁵ Angelo et al,²⁶ Foiles and Hoyt,²⁷ Voter and Chen,²⁸ and Zhou et al,²⁹ respectively, are employed. In this paper, we refer to these

potentials by the last name of the first author; for example, Mishin-EAM. For all these interatomic potentials, certain material parameters of interest are calculated and listed in Table S1, including magnitude of the Burgers vector of the Shockley partial dislocation b_p , shear modulus for the $\langle 110 \rangle\{111\}$ system μ , stable SFE e_{SF} , unstable SFE e_{USF} , stable twinning energy (also the $\Sigma 3$ CTB energy) e_T , unstable twinning energy e_{UT} , and energy of the $\Sigma 11$ STGB e_{STGB} . By employing the same potentials adopted in previous quasi-2D QC and MD simulations, we will shed light on the sensitivity of the simulated slip transfer mechanism to the interatomic potentials and the significance of large scale full 3D simulations.

RESULTS AND DISCUSSIONS

The initially straight pure screw dislocation lines bow out subject to the applied stress in the presence of traction free boundaries, obtaining mixed character. In the incoming grain, each curved dislocation splits into two Shockley partial dislocations, i.e.,

$$\frac{1}{2}a_0[110]^{in} \rightarrow \frac{1}{6}a_0[121]^{in}_{lead} + \frac{1}{6}a_0[21\bar{1}]^{in}_{trail} \quad (1)$$

Here and throughout the remainder of this paper, the superscripts “in” and “out” are used to distinguish the two grains in which the dislocation is

located, while the subscripts “lead” and “trail” refer to leading and trailing partial dislocations, respectively. In the coarse-grained domain, the two partial dislocations are separated by a stable width of 22 Å using the Mishin-EAM potential (Fig. 2a), somewhat wider than separations for a screw dislocation computed using full atomistic simulations.¹⁹ Once the dislocation migrates into the atomistic domain in the vicinity of the GBs, it obtains the same stacking fault width and core structure as those corresponding to full atomistics.^{2,14}

$\Sigma 3\{111\}$ Coherent Twin Boundary

For the $\Sigma 3\{111\}$ CTB, the leading and trailing partials must recombine in the incoming lattice prior to the interface reaction. At a shear stress of about 206 MPa for the Mishin-EAM potential,²¹ the leading partial in the incoming grain is stopped at the $\Sigma 3\{111\}$ CTB, with the stacking fault width constricting up to the point where the trailing partial also reaches the CTB, as shown in Fig. 2b. Two dislocation/CTB interaction modes are found:

- (1) For Angelo-EAM, Foiles-EAM, and Zhou-EAM potentials, the full dislocation is re-dissociated to two Shockley partials and migrates in the twin plane, i.e.,

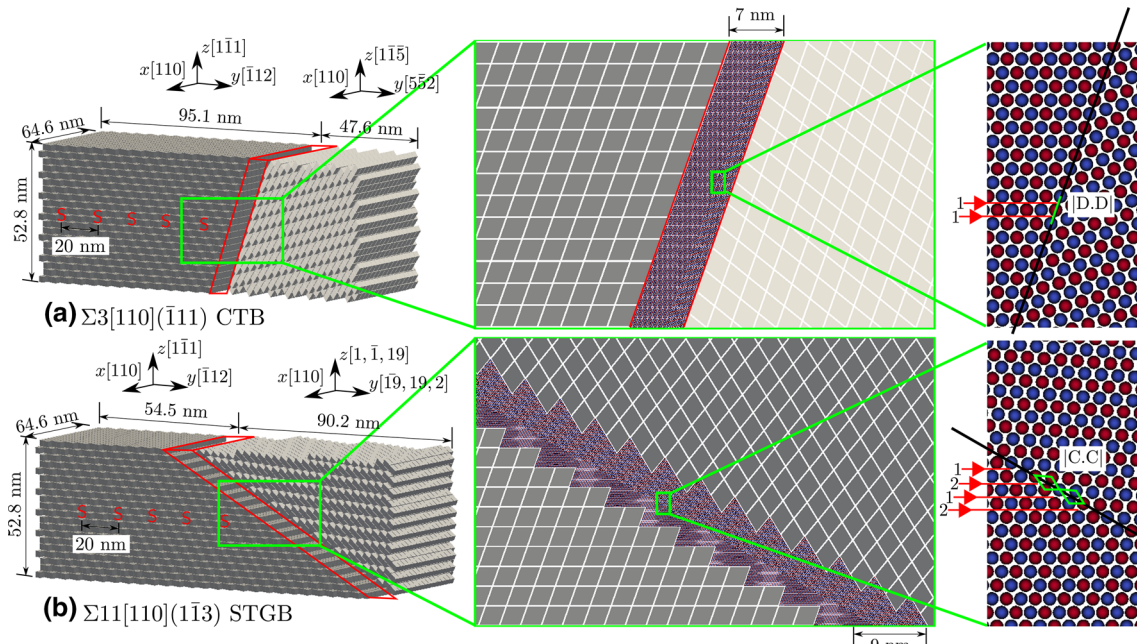


Fig. 1. Bicrystal simulation cells used to study sequential slip transfer of five ($a_0/2$) $[110](\bar{1}\bar{1}1)$ dislocations across (a) a $\Sigma 3(\bar{1}\bar{1}1)$ CTB and (b) a $\Sigma 11(1\bar{1}3)$ STGB in Ni. An atomistic domain is meshed in the vicinity of both GBs; the jagged interstices at the cell boundaries are also filled in with atoms, which are not shown here. Away from the GBs and cell boundaries are coarse-grained finite elements, each containing 2,197 atoms. All cell boundaries are assumed traction free to allow a full 3D description. Exploded views of the GB region appear in the rightmost column, where atoms in different (110) atomic layers have different colors. The top right exploded view shows that the $\Sigma 3$ CTB is composed of all D SU's, and all sites along the CTB are equivalent; the bottom right zoom-in suggests the $\Sigma 11$ STGB is composed of all C SU's, indicating that two distinct dislocation/STGB interaction sites (1 and 2) should be considered in terms of incoming dislocations.

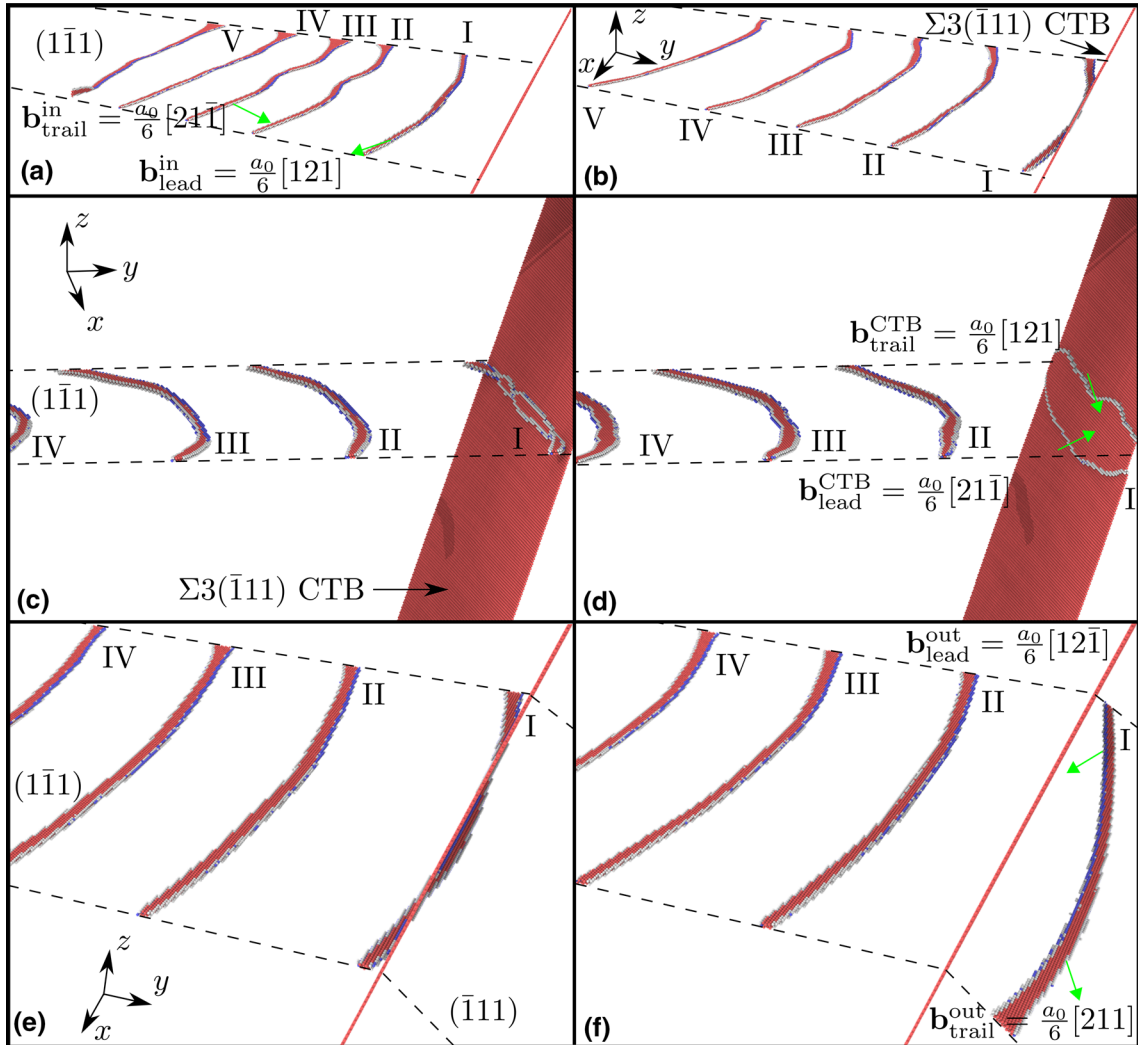


Fig. 2. Snapshots of dislocation pile-up with dominant leading screw character impinging against a $\Sigma 3(111)$ CTB. Each of the five incoming dislocations has Burgers vector $(a_0/2)[110]$. Atoms are colored by adaptive common neighbor analysis:³³ red are of hexagonal-close packed local structure, blue are body-centered cubic atoms, and all FCC atoms are deleted. In (a), five incoming dislocations approach the CTB subject to an applied shear stress. In (b), the leading dislocation is constricted at the CTB, where two Shockley partial dislocations are recombined into a full dislocation. In (c-d), with Angelo-EAM, Foiles-EAM, and Zhou-EAM potentials, the redissociated dislocation is absorbed by the CTB, with two partials gliding on the twin plane in opposite directions, according to Eq. 2. In (e-f), with Mishin-EAM and Voter-EAM potentials, the dislocation effectively cross-slips into the outgoing twinned grain via redissociation into two partials, according to Eq. 4. Views of (a-b), (c-d), and (e-f) are illustrated in (b), (c), and (e), respectively.

$$R_{\Sigma 3} \cdot \frac{1}{2} a_0 [110]^{\text{in}} \rightarrow \frac{1}{2} a_0 [110]^{\text{out}} \rightarrow \frac{1}{6} a_0 [21\bar{1}]^{\text{CTB}} + \frac{1}{6} a_0 [121]^{\text{CTB}}$$
(2)

where the slip plane (i.e., twin plane or interface plane) is $(1\bar{1}\bar{1})$; the rotation matrix between two grains is

$$R_{\Sigma 3} = \frac{1}{3} \begin{pmatrix} 1 & 2 & 2 \\ 2 & 1 & -2 \\ -2 & 2 & -1 \end{pmatrix}. \quad (3)$$

The two CTB partial dislocations then move in opposite directions along the CTB, growing the outgoing grain by one atomic layer, and eventually exiting the top/bottom traction free cell boundaries, as shown in Fig. 2c-d.

- (2) For Mishin-EAM and Voter-EAM potentials, however, instead of being absorbed by the CTB, the full dislocation is constricted and then re-dissociated into two Shockley partial dislocations which are transmitted into the outgoing grain, i.e.,

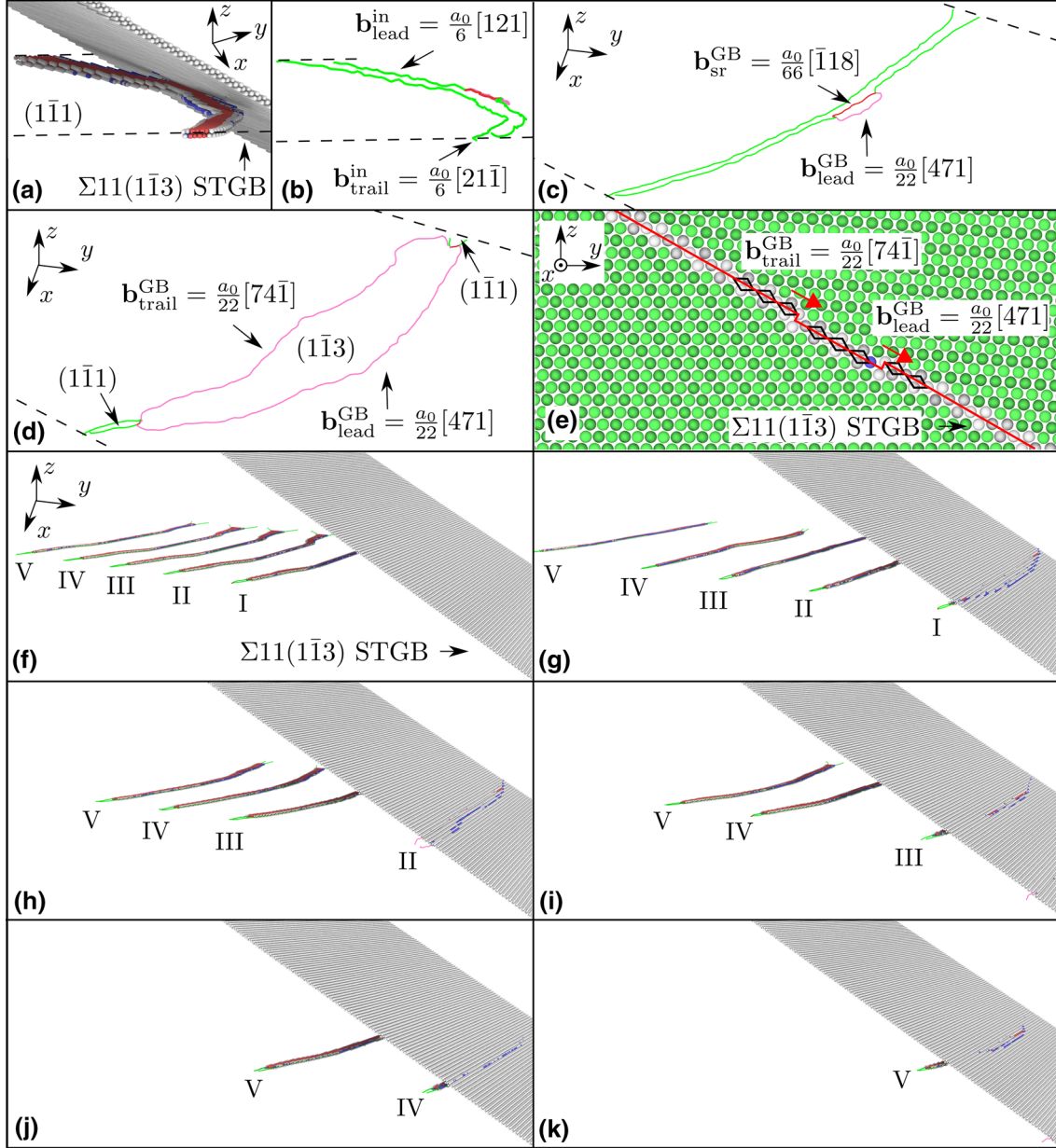


Fig. 3. Snapshots of a series of $(a_0/2)[110]$ dislocations impinging on a $\Sigma 11\{1\bar{1}3\}$ STGB. In (a) and (e–k), atoms are colored in the same manner as in Fig. 2, except that the FCC atoms (green) are not deleted in (e). In (b–d) and (f–k), a dislocation extraction algorithm³⁶ is employed to illustrate dislocations as curved lines. (a–c) are taken at the same time but with different views and/or visualization methods, where the leading partial in the incoming grain splits into a partial dislocation on the STGB and a stair-rod type of dislocation, according to Eq. 5. (d–e) are taken at the same time but with different views and visualization methods, where the trailing partial in the incoming grain reacts with the stair-rod dislocation to form another partial dislocation on the STGB, according to Eq. 6. In (g–k), the interaction mechanism for subsequent dislocations is found to be precisely the same as for the first dislocation, because each dislocation/STGB reaction does not leave residual Burgers vector in the STGB interface. Views of (a–b), (c–d), (e), and (f–k) are illustrated in (a), (c), (e), and (f), respectively.

$$\begin{aligned} R_{\Sigma 3} \cdot \frac{1}{2} a_0 [110]^{\text{in}} &\rightarrow \frac{1}{2} a_0 [110]^{\text{out}} \rightarrow \frac{1}{6} a_0 [12\bar{1}]^{\text{out}} \\ &+ \frac{1}{6} a_0 [21\bar{1}]^{\text{out}} \end{aligned} \quad (4)$$

where the slip plane in the outgoing grain is $(\bar{1}11)$, on which the outgoing dislocation continues migrating until exiting the rightmost traction free cell boundary, as shown in Fig. 2e–f.

Reactions predicted by employing Mishin-EAM and Angelo-EAM potentials in CAC agree with previous MD simulations of a screw dislocation interacting with a $\Sigma 3$ CTB in Ni using the same potentials.^{21,22} In both modes of the dislocation/GB interactions, the two partial dislocations exchange their order after encountering the CTB due to the twin symmetry.² Since each dislocation/CTB reaction does not leave residual Burgers vector in the

CTB interface, the interaction mechanism for subsequent dislocations is found to be precisely the same as for the first dislocation. The minimum stress for each dislocation transmission/absorption, however, increases as there are fewer dislocations residing in the incoming pile-up. By comparison, a minimum applied shear stress of 480 MPa is needed for a single pure screw dislocation to be transmitted across the CTB using the Mishin-EAM potential,²¹ which is more than twice the 206 MPa stress level corresponding to the case of the pileup.

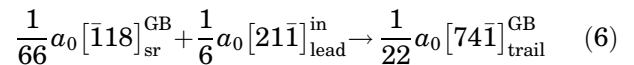
Based on MD simulations of screw dislocation/CTB interactions, Jin et al.²² employed two dimensionless parameters, i.e., (1) the resistance encountered by a screw dislocation to be transmitted through the CTB, $R = (e_{\text{USF}} - e_{\text{SF}})/\mu b_p$, and (2) the resistance to cross-slip on the CTB plane, $R' = (e_{\text{UT}} - e_{\text{SF}})/\mu b_p$. Based on the criteria of Jin et al.,²² dislocation absorption by a $\Sigma 3$ CTB is predicted to occur if $R/R' = (e_{\text{USF}} - e_{\text{SF}})/(e_{\text{UT}} - e_{\text{SF}})$ is negative; otherwise, a dislocation would be transmitted through the CTB. For all five EAM potentials employed in this paper, R/R' is between 1.01 and 1.08, whereas dislocation absorption is observed with three potentials. Thus, this criterion is not adequate to discriminate between screw dislocation absorption and transmission upon encountering a CTB.²¹ Based on MD simulations, Chassagne et al.²¹ proposed a new slip transfer criterion, asserting that materials with a low $e_{\text{SF}}/\mu b_p$ have widely dissociated dislocations with a high constriction stress that favors transmission over absorption. In our simulations, the Voter-EAM potential has the smallest $e_{\text{SF}}/\mu b_p$ and gives dislocation transmission, while the Foiles-EAM potential, which has the largest $e_{\text{SF}}/\mu b_p$, results in dislocation absorption. The criterion of Chassagne et al.,²¹ however, doesn't sufficiently discriminate between dislocation transmission and absorption for the $\Sigma 3$ CTB; although the Mishin-EAM potential has a higher $e_{\text{SF}}/\mu b_p$ value than that of the Zhou-EAM potential, the incoming dislocation is transmitted across the CTB using the former but is absorbed by the CTB using the latter, at the same applied stress level. Inspection of Table S1 shows that the value of R itself, which is related to the nucleation of the trailing partial dislocation according to Rice's theory,³⁸ can be used to predict dislocation/CTB reactions: Mishin-EAM and Voter-EAM potentials, which have the largest R , yield dislocation transmission, while the other EAM potentials with smaller R predict dislocation absorption. It is, however, difficult to forecast what the dislocation/CTB reaction would be in a full *ab initio* simulation, because the *ab initio* value of R ³⁹ is smaller than that of the Mishin-EAM potential, which yields dislocation transmission, but larger than that of the Zhou-EAM potential, which results in dislocation absorption. Given that all these criteria are directly related to the SFEs, our work highlights the significance of choosing EAM potentials with appropriate GSFE values for problems involving behavior of dislocations.

$\Sigma 11\{113\}$ Symmetric Tilt Grain Boundary

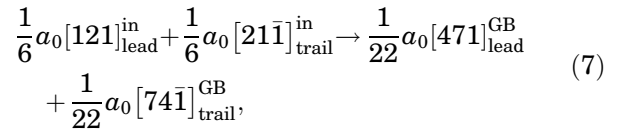
At a shear stress of 257 MPa, unlike the case of the $\Sigma 3$ CTB, the full dislocation is not necessarily recombined at the $\Sigma 11\{113\}$ STGB. The leading partial in the incoming grain first splits into a leading partial dislocation belonging to the displacement shift complete lattice of the STGB and a stair-rod type of dislocation (Fig. 3a–c), i.e.,



where the subscript "sr" refers to the stair-rod type of dislocation, which then reacts with the trailing partial dislocation in the incoming grain (Fig. 3d), i.e.,



where the slip plane for the STGB partial dislocations in terms of the incoming grain is $(1\bar{1}3)$. The overall reaction in Eqs. 5 and 6 is



which is energetically favorable according to Frank's rule,¹ since the original $b_{\text{lead}}^2 + b_{\text{trail}}^2 = (1/3)a_0^2$ while the resultant $b_{\text{lead}}^2 + b_{\text{trail}}^2 = (3/11)a_0^2$. The two STGB partials on the RHS in Eq. 7, with Burgers vectors parallel to the GB plane, locally grow the outgoing grain by one atomic layer. The force per unit length on a partial dislocation can be obtained by the Peach-Koehler (PK) formula, $\mathbf{F} = (\mathbf{b}_p \cdot \boldsymbol{\sigma}) \times \mathbf{t}$, where $\boldsymbol{\sigma}$ is the applied shear stress tensor whose only two non-zero components are σ_{xz} and σ_{zx} , both of which are negative, \mathbf{t} is the unit tangent vector of the dislocation line along the negative x axis, and \mathbf{b}_p should be transformed to the spatial Burgers vector. It is found that the PK forces drive the two STGB partials, separated by 101A, to migrate in the same positive y (and negative z) direction, before they eventually exit the bottom traction free surface. We remark that a different applied stress tensor may alter the STGB partial dislocation migration, as suggested by Dewald and Curtin.⁹ For the same $\Sigma 11\{113\}$ STGB, the two-step dislocation absorption in Eqs. 5 and 6 was observed for edge dislocations in a QC simulation in Ni,²⁴ as well as edge and 60° mixed type dislocations in CADD simulations in Al,^{9,40} but not for screw dislocations in a CADD simulation in Al,¹⁰ an MD simulation in Cu,⁴¹ or a high resolution TEM experiment in Ni,⁴² in which only reactions according to Eq. 7 were reported. This is probably due to an insufficient fidelity in monitoring the computational/experimental output for Cu and Ni. Similar to the $\Sigma 3$ CTB, the interaction mechanism for subsequent dislocations is found to be precisely the same as for the first dislocation, because each dislocation/

STGB reaction does not leave residual Burgers vector in the STGB interface, as shown in Fig. 3f–k. All five EAM potentials in the case of two interaction sites predict similar results.

A Comparison Between the Two GBs

In both $\Sigma 3\{111\}$ CTB and $\Sigma 11\{113\}$ STGB, dislocation absorption is manifested by a step height of one interplanar spacing in the GB, which is restored by the trailing partial dislocation if it moves in the same direction as the leading partial. With certain interatomic potential fits, both GBs act as sinks for lattice dislocations, absorbing dislocations from one grain and transferring to GB-mediated structural evolution. For Mishin-EAM and Voter-EAM potentials, however, the $\Sigma 3$ CTB acts as a barrier to dislocation motion, followed by transmission of full dislocations across the CTB under an applied stress; in this case, plasticity is apparently governed by lattice dislocation processes rather than CTB processes.

Based on MD simulations in Ni involving an isolated dislocation in a confined volume using the Foiles-EAM potential, Sangid et al.²⁰ proposed that GBs with lower energy offer a stronger barrier against slip transmission. In their work, dislocations of either pure edge or mixed type with dominant leading edge character were employed, which are known to be transmitted through most GBs.⁴³ However, it raises a question whether the same model holds for incoming mixed dislocations with dominant leading screw character, which may be absorbed by GBs.² In our simulations, all five EAM potentials yield a much higher energy for the $\Sigma 11$ STGB (e_{STGB}) than the $\Sigma 3$ CTB (e_{T}). Angelo-EAM, Foiles-EAM, and Mishin-EAM potentials predict absorption of mixed type dislocations by both $\Sigma 3$ CTB and $\Sigma 11$ STGB, and thus it is difficult to determine which GB acts as a stronger barrier to slip transmission in these cases. On the other hand, Mishin-EAM and Voter-EAM potentials predict transmission of dislocations across a $\Sigma 3$ CTB (with a low excess interface energy) but absorption of the same dislocations by a $\Sigma 11$ STGB (with a high energy), in violation of the assertion of Sangid et al.²⁰ We remark that unlike the work of Sangid et al.²⁰ which employed the same GB plane with respect to the applied loading while varying the dislocation plane/character angle, our CAC simulations ensure the same dislocation plane/character angle while varying the GB plane for different GBs. This suggests that the GB energy may serve as an indicator for slip transmission for particular types of dislocations, GB planes, and certain fits to interatomic potentials.⁴² In other words, applicability of dislocation/GB interaction criteria derived from limited studies may be limited.

CONCLUSION

In this paper, 0 K quenched dynamic CAC simulations with periodic energy minimization are employed to study 3D sequential slip transfer across

a $\Sigma 3\{111\}$ CTB and a $\Sigma 11\{113\}$ STGB using five different fits to the EAM interatomic potential in Ni to concern the dependence of the simulated slip transfer responses on the interatomic potential. A series of curved dislocations are driven toward both GBs subject to an applied shear stress. For the $\Sigma 3$ CTB, the leading screw segment is transmitted into the twinned grain using two interatomic potentials, while it is absorbed and glides on the CTB when the other three potentials are employed. In both reactions, each dislocation always follows the recombination-redissociation process, without forming any CTB dislocations in the process of recombination. For the $\Sigma 11$ STGB, however, all five EAM potential fits predict dislocation absorption, during which the leading partial dislocation in the incoming grain splits into a STGB partial dislocation and a stair-rod type dislocation, which subsequently reacts with the trailing partial dislocation in the incoming grain to form another STGB partial dislocation. It is also found that certain slip transmission criteria in the literature, which are proposed based on limited studies, do not adequately predict the dislocation/GB reaction for different GBs and interatomic potentials.

ACKNOWLEDGEMENTS

These results are based upon work supported by the National Science Foundation as a collaborative effort between Georgia Tech (CMMI-1232878) and University of Florida (CMMI-1233113). Any opinions, findings, and conclusions or recommendations expressed in this material are those of the authors and do not necessarily reflect the views of the National Science Foundation. LX acknowledges the support from the Department of Energy, Office of Basic Energy Sciences under Award Number DE-SC0006539. The work of LX was also supported in part by the National Science Foundation under Award Number CMMI-1536925. The authors thank Dr. Dengke Chen and Dr. Benjamin Szajewski for helpful discussions, Dr. Stephen M. Foiles for providing the tabulated Foiles-EAM potential file, and Dr. Alexander Stukowski for providing the dislocation extraction algorithm code. This work used the Extreme Science and Engineering Discovery Environment (XSEDE), which is supported by National Science Foundation Grant Number ACI-1053575.

ELECTRONIC SUPPLEMENTARY MATERIAL

The online version of this article (doi:[10.1007/s11837-017-2302-1](https://doi.org/10.1007/s11837-017-2302-1)) contains supplementary material, which is available to authorized users.

REFERENCES

1. J.P. Hirth and J. Lothe, *Theory of Dislocations* (Hoboken: Wiley, 1982).

2. S. Xu, L. Xiong, Y. Chen, and D.L. McDowell, *npj Comput. Mater.* 2, 15016 (2016).
3. J. Wang, *JOM* 67, 1515 (2015).
4. D.E. Spearot and M.D. Sangid, *Curr. Opin. Solid State Mater. Sci.* 18, 188 (2014).
5. J. Kacher and I.M. Robertson, *Acta Mater.* 60, 6657 (2012).
6. J. Kacher, B.P. Eftink, B. Cui, and I.M. Robertson, *Curr. Opin. Solid State Mater. Sci.* 18, 227 (2014).
7. D.L. McDowell, *Int. J. Plast.* 26, 1280 (2010).
8. B. Liu, D. Raabe, P. Eisenlohr, F. Roters, A. Arsenlis, and G. Hommes, *Acta Mater.* 59, 7125 (2011).
9. M. Dewald and W. Curtin, *Model. Simul. Mater. Sci. Eng.* 19, 055002 (2011).
10. M.P. Dewald and W.A. Curtin, *Philos. Mag.* 87, 4615 (2007).
11. W. Yu and Z. Wang, *Comput. Mater. Sci.* 87, 150 (2014).
12. Y. Chen, *J. Chem. Phys.* 130, 134706 (2009).
13. L. Xiong, G. Tucker, D.L. McDowell, and Y. Chen, *J. Mech. Phys. Solids* 59, 160 (2011).
14. S. Xu, R. Che, L. Xiong, Y. Chen, and D.L. McDowell, *Int. J. Plast.* 72, 91 (2015).
15. L. Xiong, S. Xu, D.L. McDowell, and Y. Chen, *Int. J. Plast.* 65, 33 (2015).
16. L. Xiong, J. Rigelesaiyin, X. Chen, S. Xu, D.L. McDowell, and Y. Chen, *Acta Mater.* 104, 143 (2016).
17. S. Xu, L. Xiong, Y. Chen, and D.L. McDowell, *Acta Mater.* 122, 412 (2017).
18. S. Xu, L. Xiong, Y. Chen, and D.L. McDowell, *Scr. Mater.* 123, 135 (2016).
19. S. Xu, L. Xiong, Y. Chen, and D.L. McDowell, *J. Mech. Phys. Solids* 96, 460 (2016).
20. M.D. Sangid, T. Ezaz, H. Sehitoglu, and I.M. Robertson, *Acta Mater.* 59, 283 (2011).
21. M. Chassagne, M. Legros, and D. Rodney, *Acta Mater.* 59, 1456 (2011).
22. Z.H. Jin, P. Gumbsch, E. Ma, K. Albe, K. Lu, H. Hahn, and H. Gleiter, *Scr. Mater.* 54, 1163 (2006).
23. Z.H. Jin, P. Gumbsch, K. Albe, E. Ma, K. Lu, H. Gleiter, and H. Hahn, *Acta Mater.* 56, 1126 (2008).
24. W. Yu and Z. Wang, *Philos. Mag.* 94, 2224 (2014).
25. Y. Mishin, D. Farkas, M.J. Mehl, and D.A. Papaconstantopoulos, *Phys. Rev. B* 59, 3393 (1999).
26. J.E. Angelo, N.R. Moody, and M.I. Baskes, *Model. Simul. Mater. Sci. Eng.* 3, 289 (1995).
27. S.M. Foiles and J.J. Hoyt, *Acta Mater.* 54, 3351 (2006).
28. A.F. Voter and S.P. Chen, *Mater. Res. Soc. Symp. Proc.* 82, 175 (1987).
29. X.W. Zhou, R.A. Johnson, and H.N.G. Wadley, *Phys. Rev. B* 69, 144113 (2004).
30. J.B. Liu, D.D. Johnson, and A.V. Smirnov, *Acta Mater.* 53, 3601 (2005).
31. S. Xu, L. Xiong, Q. Deng, and D.L. McDowell, *Int. J. Solids Struct.* 90, 144 (2016).
32. S. Xu (Ph.D. Dissertation, Georgia Institute of Technology, Atlanta, GA, USA, 2016).
33. W. Schroeder, K. Martin, and B. Lorensen, *The Visualization Toolkit: An Object Oriented Approach to 3D Graphics* (Clifton Park: Kitware, 2003).
34. A. Stukowski, *Model. Simul. Mater. Sci. Eng.* 18, 015012 (2010).
35. A. Stukowski, *Model. Simul. Mater. Sci. Eng.* 20, 045021 (2012).
36. A. Stukowski, V.V. Bulatov, and A. Arsenlis, *Model. Simul. Mater. Sci. Eng.* 20, 085007 (2012).
37. J. Towns, T. Cockerill, M. Dahan, I. Foster, K. Gaither, A. Grimshaw, V. Hazlewood, S. Lathrop, D. Lifka, G.D. Peterson, R. Roskies, J.R. Scott, and N. Wilkins-Diehr, *Comput. Sci. Eng.* 16, 62 (2014).
38. J.R. Rice, *J. Mech. Phys. Solids* 40, 239 (1992).
39. S. Kibey, J.B. Liu, D.D. Johnson, and H. Sehitoglu, *Acta Mater.* 55, 6843 (2007).
40. M.P. Dewald and W.A. Curtin, *Model. Simul. Mater. Sci. Eng.* 15, S193 (2007).
41. B.J. Pestman, JThM de Hosson, V. Vitek, and F.W. Schapink, *Scr. Metall.* 23, 1431 (1989).
42. L. Priester, S. Poulat, B. Décamps, and J. Thibault, *Mater. Res. Soc. Symp. Proc.* 652, 1 (2001).
43. L.C. Lim and R. Raj, *Acta Metall.* 33, 1577 (1985).